 doi:10.20944/preprints201901.0243.v1

Article

Distributed orbit determination for Global Navigation Satellite System with inter-satellite link

Yuanlan Wen [1]*, Jun Zhu [2], Youxing Gong [3], Qian Wang[1], Xiufeng He [1,]*

[1] School of Earth Sciences and Engineering, Hohai University, Nanjing 210098, China; wwwgwyl@126.com(Y.W.); wqaloha@139.com(Q.W.); xfhe@hhu.edu.cn(X.H)
[2] Xi'an Satellite Control Center, Xi'an 710043, China; zhujun9306@126.com (J.Z)
[3] Undergraduate School, National University of Defense Technology, Changsha 410073, China; 13874804178@139.com(Y.G)
* Correspondence: wwwgwyl@126.com; xfhe@hhu.edu.cn; Tel.: +86-25-83786961

Abstract: To keep the global navigation satellite system functional during extreme conditions, it is a trend to employ autonomous navigation technology with inter-satellite link. As in the newly built BeiDou system (BDS-3) equipped with Ka-band inter-satellite links, every individual satellite has the ability of communicating and measuring distances among each other. The system also has less dependence on the ground stations and improved navigation performance. Because of the huge amount of measurement data, centralized data processing algorithm for orbit determination is suggested to be replaced by a distributed one in which each satellite in the constellation is required to finish a partial computation task. In current paper, the balanced extended Kalman filter algorithm for distributed orbit determination is proposed and compared with whole-constellation centralized extended Kalman filter, iterative cascade extended Kalman filter, and increasing measurement covariance extended Kalman filter. The proposed method demands a lower computation power however yields results with a relatively good accuracy.

Keywords: Inter-satellite link; Whole-constellation centralized extended Kalman filter; Distributed orbit determination; Iterative cascade extended Kalman filter; Increased measurement covariance extended Kalman filter; Balanced extended Kalman filter

1. Introduction

For global navigation satellite system (GNSS), currently, the master control station (MCS) collects the satellite to monitor station measurement data, estimates the satellite ephemeris and clock offsets, and generates a time stream of navigation messages. The messages are then uploaded to satellites by ground antennas to broadcast to the user community [1]. However, the MCS as well as the other ground-based segments including monitor stations and ground antennas have the risk of destruction during a warfare or natural disaster. This is the case especially for the monitor stations which distributed globally for increasing the accuracy of satellite orbit determination [2]. In order to enhance the viability of the satellite navigation systems under the potentially fatal conditions, as early as in 1980s, the autonomous navigation techniques using inter-satellite link (ISL) measurements without supports from the MCS were investigated for the global positioning system (GPS) [3]. If the ISL measurement was the unique source for orbit determination and time synchronization, the datum mark would be insufficient [4]. This problem can be addressed by setting up a few ground anchorage stations (GASs) which provide reference coordinate system and time system [5]. Combining both the ISL and satellite-to-GAS measurements, the autonomous navigation system has several features: firstly, the data processing will be completed by satellite onboard computers rather than the MCS; secondly, the GASs can be considered as pseudo-satellites; and finally, the globally allocated monitor stations can be replaced by a few domestic GASs [3].

 doi:10.20944/preprints201901.0243.v1

Centralized data processing technique, which is widely applied in current autonomous navigation constellation, collects the ISL and satellite-to-GAS measurement data, combines all the satellite state vectors (including satellite orbit, clock error parameters, etc.) into one matrix, and computes the optimal state vector for each satellite by a central satellite on-board computer. As results, the associated state vector covariance matrix could be very large, the method requires a vast computation power [6]. It is worth to mention that, in this case, every satellite is observed indirectly by other satellites.

Whereas in distributed data processing algorithm, the computation is broken down and assigned to each satellite. Each satellite is required to deal with self-related ISL measurements and local state vectors. In this way, the number of measurement equations and dimension of the state vectors are reduced. As a result, the computational amount of the whole system are decreased considerably. Moreover, the accuracy of the orbit ephemeris and clock offsets calculated by distributed data processing method could have the same level to the results of centralized data processing.

With the measurements from ISLs and satellite-to-GASs, the autonomous navigation constellation constitutes an extremely complex system. Each satellite has to finish the task of ISL measurement, data processing, and communicating. A practical algorithm for autonomous orbit determination is still under development. Based on the method of iterative cascade extended Kalman filter (ICEKF) and increased measurement covariance extended Kalman filter (IMCEKF), a new distributed method, balanced extended Kalman filter (BEKF), is proposed in this paper. Together with whole-constellation centralized extended Kalman filter (WCCEFK), four different autonomous navigation algorithms are conducted in simulations for comparisons of accuracy and computation loads.

2. Overview of Orbit Determination Algorithms

Ananda [7] proposed the framework of autonomous navigation system without a MCS at the first time and validated the system by simulations. Rajan [3] introduced various autonomous navigation algorithms and presented preliminary on-orbit experiment results.

In the designing of the GPS Block IIR, the ISLs, programmable microprocessors, and redundant management were carried out. The following two major features are critical to ensure high precision autonomous navigation [3, 7]:

- The ISL communications and measurements in UHF band.
- A high-precision autonomous navigation algorithm which is adapted to the computing capacity of the satellite on-board computers;

A time division multiple access (TDMA) system, which has two frames, was employed for ranging and data transmission. In ranging frame, each satellite is assigned a 1.5-second slot to make pseudo-range (PR) measurements with the visible satellites. Two frequencies were used in the measurement for ionospheric delay corrections. In data frame, a 1.5-second slot was appointed to each satellite to transmit data includes the PR measurements, the estimated satellite state vector, and the associated covariance matrix to all visible satellites.

The GPS Block IIF follows the design of the GPS Block IIR and improves the performance of ISL measurements and on-board data processing. Without contacting with the ground system, Block IIF can operate about 60 days in the autonomous navigation mode and provide navigation messages which are corrected by ISL measurements with a 3-meter user range error (URE) (URE is a root mean square value and does not consider the impact of the polar motion and UT1). However, it is difficult to establish a precise prediction system because of the irregular polar motion and uncertain UT1. Therefore, in autonomous navigation mode, the URE is far greater than 3 meters in a 60-day duration [8].

For the GPS III, each satellite in the constellation will have the ability of ISL measurements and communications. It is designed that once there are enough number of satellites in orbit, the GPS constellation will be able to operate autonomously in wartime, but currently they are still under investigation [9].

Preprints (www.preprints.org) | NOT PEER-REVIEWED | Posted: 24 January 2019 doi:10.20944/preprints201901.0243.v1

Galileo navigation system is also planned to employ autonomous navigation algorithm based on ISLs [10]. Spatial orientation problem is solved by the combination of the ISL and satellite-to-ground measurements. The simulation for Galileo system showed that URE is on the level of decimeters [10], which is better than that of GPS.

For the distributed navigation algorithms, several techniques including iterative cascade extended Kalman filter (ICEKF), increased measurement covariance EKF (IMCEKF), and Schmidt-Kalman Filter (SKF) are discussed by Schmidt, Park and Ferguson [11-13]. The ICEKF is employed to processes a large number of space-borne GPS measurement data and a small quantity of ISL measurement data for low-Earth orbit formation flying satellites. In this method, the computation process will iterate for 3 to 4 times for convergence and a good orbit accuracy is presented. For the method of IMCEKF, amendments are made based on ICEKF and it presents a better performance. On the other hand, the SKF yield results with a less accuracy compared to IMCEKF while processing the GNSS ISL measurement data [4]. Recently, International Association of Geodesy (IAG) initiates a GPS Dancer project which develops a distributed data processing algorithm to analyze the precision of the GPS [14].

In China, distributed orbit determination and time synchronization algorithms based on ISL measurements were studied [15-21]. The distributed autonomous ephemeris updating were discussed for navigation satellites [22]. There are also many researches on developing higher precision orbit determination methods for new BeiDou (BDS-3) experimental satellites in the literature [23-26]. Currently, the developments for autonomous orbit determination, time synchronization, and autonomous operation and management are wildly investigated. More progress on designing an efficient distributed data processing algorithm, however, needs to be made.

3. Fundamental Equations for Measurement and Motion

3.1. Equations for Measurement

The position vectors, $\vec{r}^{\,i} = [x^i \quad y^i \quad z^i]^{\mathrm{T}}$, velocity vectors, $\vec{v}^{\,i} = [v_x^i \quad v_y^i \quad v_z^i]^{\mathrm{T}}$, and dynamic parameter vector, x_D^i, consititue the state vector which need to be estimated:

$$\boldsymbol{X}^i = \left[\vec{\boldsymbol{r}}^{\,iT} \;\; \vec{\boldsymbol{v}}^{\,iT} \;\; x_D^{i\,T}\right]^{\mathrm{T}} \tag{1}$$

In here, the superscript, T, denotes the transpose of a matrix, and the superscript, i, denotes that it is for the ith satellite. The reference values for the state vector are stored in $\boldsymbol{X}^{i^*}$, and the improving values for the state vector are written in:

$$\delta \boldsymbol{x}^i = \boldsymbol{X}^i - \boldsymbol{X}^{i^*} \tag{2}$$

After correcting the hardware delay, ionospheric delay, relativistic effect, multi-path effect, and the antenna phase center offset [4], two one-way ISL PRs between the ith satellite and jth satellite need to be translated into a same measurement epoch (e.g. ranging frame epoch *t*). The PR equations are:

$$\rho^{i\to j}(t) = c\cdot[\delta t^j(t) - \delta t^i(t)] + d(\boldsymbol{X}^j(t), \boldsymbol{X}^i(t)) + \varepsilon^{i\to j}(t) \tag{3}$$

$$\rho^{j\to i}(t) = c\cdot[\delta t^i(t) - \delta t^j(t)] + d(\boldsymbol{X}^j(t), \boldsymbol{X}^i(t)) + \varepsilon^{j\to i}(t) \tag{4}$$

where, c is the speed of light, $\delta t^i(t)$ and $\delta t^j(t)$ are clock errors for the ith satellite and the jth satellite, $\varepsilon^{i\to j}(t)$ and $\varepsilon^{j\to i}(t)$ are the measurement errors, $d(\boldsymbol{X}^j(t), \boldsymbol{X}^i(t)) = \sqrt{(x^i - x^j)^2 + (y^i - y^j)^2 + (z^i - z^j)^2}$ is the geometric distance between the two satellites. Combining equations (3) and (4), distance measurement equation that only contains orbit parameter is derived as:

Preprints (www.preprints.org) | NOT PEER-REVIEWED | Posted: 24 January 2019 doi:10.20944/preprints201901.0243.v1

$$\rho^{ij}(t)=\left[\rho^{j\to i}(t)+\rho^{i\to j}(t)\right]/2=d(\boldsymbol{X}^{j}(t),\boldsymbol{X}^{j}(t))+\varepsilon^{ij}(t) \tag{5}$$

where, $\varepsilon^{ij}(t_k)=[\varepsilon^{i\to j}(t_k)+\varepsilon^{j\to i}(t_k)]/2$. Subtracting equation (4) from equation (3), time measurement equation that only contains clock error parameters is deduced as:

$$\rho^{ij}_{clock}(t)=\left[\rho^{j\to i}(t)-\rho^{i\to j}(t)\right]/2=c\cdot[\delta t^{j}(t)-\delta t^{i}(t)]+\left[\varepsilon^{j\to i}(t)-\varepsilon^{i\to j}(t)\right]/2 \tag{6}$$

Following the steps above, the distance measurements and the clock bias measurements are decoupled, the orbit ephemeris and clock offsets can therefore be estimated independently.

Linearizing equation (5) with Taylor expansion at the reference state vector $\boldsymbol{X}^{i*}$ and $\boldsymbol{X}^{j*}$ yields:

$$\rho^{ij}(t)=d\left(\boldsymbol{X}^{i*},\boldsymbol{X}^{j*}\right)+\left.\frac{\rho^{ij}(t)}{\partial\boldsymbol{X}^{i}}\right|_{\boldsymbol{X}^{i*}}\delta x^{i}+\left.\frac{\rho^{ij}(t)}{\partial\boldsymbol{X}^{j}}\right|_{\boldsymbol{X}^{j*}}\delta x^{j}+\cdots+\varepsilon^{ij}(t) \tag{7}$$

After that, equation (7) is converted into a linear measurement equation:

$$z^{ij}(t)=\boldsymbol{H}^{i}\delta\boldsymbol{x}^{i}(t)+\boldsymbol{H}^{j}\delta\boldsymbol{x}^{j}(t)+\varepsilon^{ij}(t) \tag{8}$$

where $z^{ij}(t)=\rho^{ij}(t)-d\left(\boldsymbol{X}^{i*},\boldsymbol{X}^{j*}\right)$ is the innovation, $\boldsymbol{H}^{i}$ and $\boldsymbol{H}^{j}$ are the measurement matrices.

$$H^{i}=\left.\frac{\rho^{ij}(t)}{\partial\boldsymbol{X}^{i}}\right|_{\boldsymbol{X}^{i*}}=\left[\begin{array}{ccc}\dfrac{x^{i}-x^{j}}{d\left(\boldsymbol{X}^{i*},\boldsymbol{X}^{j*}\right)} & \dfrac{y^{i}-y^{j}}{d\left(\boldsymbol{X}^{i*},\boldsymbol{X}^{j*}\right)} & \dfrac{z^{i}-z^{j}}{d\left(\boldsymbol{X}^{i*},\boldsymbol{X}^{j*}\right)}\end{array}\right]_{\boldsymbol{X}^{i*}} \tag{9}$$

$$H^{j}=\left.\frac{\rho^{ij}(t)}{\partial\boldsymbol{X}^{j}}\right|_{\boldsymbol{X}^{j*}}=-H^{i} \tag{10}$$

Similarly, GAS can be considered as a pseudo-satellite. The PR needs to be corrected by an extra tropospheric delay compared to a normal satellite. Distance measurement equation that contains orbit parameters between gth GAS and ith satellite is derived as

$$\rho^{ig}(t)=\left[\rho^{g\to i}(t)+\rho^{i\to g}(t)\right]/2=d(\boldsymbol{X}^{i}(t),\boldsymbol{X}^{g}(t))+\varepsilon^{ig}(t) \tag{11}$$

In the equation (11) , the array of state parameters of GAS $\boldsymbol{X}^{g}(t)$ is known, only the state vector of ith satellite is unknown. The reference ground coordinate is hence introduced into the satellite state by equation (11), this overcomes the lack of the datum mark in data processing while only ISL measurements are utilized. The current linearized measurement equation which is similar to equation (8) becomes:

$$z^{ig}(t\ )=\boldsymbol{H}^{i}\delta\boldsymbol{x}^{i}(t)+\varepsilon^{ig}(t) \tag{12}$$

3.2. Equations for Motion

Satellites can be affected by a variety of factors when operated in orbit. For navigation satellites in here, only the gravitational forces, solar radiation pressure, and relativistic effects are considered [27]. The gravitational forces include the attractions from the earth, the moon, and other planets in the solar system. The dynamic equation for the ith satellite can be written as:

$$\dot{\boldsymbol{X}}^{i}(t)=f^{c}(\boldsymbol{X}^{i},\boldsymbol{w}^{i}) \tag{13}$$

Preprints (www.preprints.org) | NOT PEER-REVIEWED | Posted: 24 January 2019 doi:10.20944/preprints201901.0243.v1

where f^c is a continuous function, $\boldsymbol{w}^i$ is the system disturbances that has the following properties:

$$E\left[\boldsymbol{w}^i(t)\right]=0,\quad E\left[\boldsymbol{w}^i(t)(\boldsymbol{w}^i(\tau))^{\mathrm{T}}\right]=\begin{cases}\boldsymbol{Q}^i(t) & t=\tau\\ 0 & t\neq\tau\end{cases} \tag{14}$$

$E[\cdot]$ denotes the expected value and $\boldsymbol{Q}^i(t)$ is a covariance matrix which is symmetric, non-negative, and definite. In here, the system disturbances are simulated by Gaussian white noise. Because the continuous function f^c and the system disturbance $\boldsymbol{w}^i$ is not coupled with each other, Equation (13) can be written as:

$$\dot{\boldsymbol{X}}^i(t)=\mathcal{F}^{\mathrm{c}}(\boldsymbol{X}^i(t))+\boldsymbol{G}\boldsymbol{w}^i \tag{15}$$

in which $\boldsymbol{G}=\left[\boldsymbol{0}\quad\boldsymbol{I}\quad\boldsymbol{0}\right]^{\mathrm{T}}$ is coefficient matrix, and the $\boldsymbol{I}$ is the identity matrix, the $\boldsymbol{0}$ is the zero matrix. Equation (15) is then linearized by Taylor expansion at the reference state vector $\boldsymbol{X}^{i*}$ as:

$$\dot{\boldsymbol{X}}^i(t)=\mathcal{F}^{\mathrm{c}}(\boldsymbol{X}^{i*}(t))+\left.\frac{\partial\mathcal{F}^{\mathrm{c}}(\boldsymbol{X}^i)}{\partial\boldsymbol{X}^i}\right|_{\boldsymbol{X}^{i*}}(\boldsymbol{X}^i(t)-\boldsymbol{X}^{i*}(t))+\cdots+\boldsymbol{G}\boldsymbol{w}^i \tag{16}$$

From equation above, the state increments are then derived as:

$$\delta\dot{\boldsymbol{x}}^i(t)=\boldsymbol{F}(t)\delta\boldsymbol{x}^i(t)+\boldsymbol{G}\boldsymbol{w}^i \tag{17}$$

where $\delta\dot{\boldsymbol{x}}=\dot{\boldsymbol{X}}-\mathcal{F}^{\mathrm{c}}(\boldsymbol{X}^{i*}(t))$ and $\boldsymbol{F}(t)$ is the dynamic partial derivative matrix[6]:

$$\boldsymbol{F}(t)=\left.\frac{\partial\mathcal{F}^{\mathrm{c}}(\boldsymbol{X})}{\partial\boldsymbol{X}}\right|_{\boldsymbol{X}^*}=\left.\begin{bmatrix}0 & \boldsymbol{I} & 0\\ \dfrac{\partial\mathcal{F}^{\mathrm{c}}}{\partial\boldsymbol{r}} & \dfrac{\partial\mathcal{F}^{\mathrm{c}}}{\partial\dot{\boldsymbol{r}}} & \dfrac{\partial\mathcal{F}^{\mathrm{c}}}{\partial\boldsymbol{p}_{\mathrm{D}}}\\ 0 & \boldsymbol{0} & 0\end{bmatrix}\right|_{\boldsymbol{X}^*} \tag{18}$$

The equation (17) is the state equation of the stochastic linear continuous systems and its general solution is:

$$\delta\boldsymbol{x}^i(t)=\boldsymbol{\Phi}^i(t,t_0)\delta\boldsymbol{x}_0^i(t)+\boldsymbol{G}\int_{t_0}^{t}\boldsymbol{\Phi}^i(t,\tau)\boldsymbol{w}^i(\tau)\mathrm{d}\tau \tag{19}$$

in which, $\boldsymbol{\Phi}^i(t,t_0)$ is the system state transition matrix and is the solution of the following equations:

$$\dot{\boldsymbol{\Phi}}^i(t,t_0)=\boldsymbol{F}(t)\boldsymbol{\Phi}^i(t,t_0),\quad\boldsymbol{\Phi}^i(t_0,t_0)=\boldsymbol{I} \tag{20}$$

where $\boldsymbol{I}$ is the identity matrix with the same dimensions as dynamics matrix, $\boldsymbol{F}(t)$.

The state transition matrix $\boldsymbol{\Phi}^i(t,t_0)$ has the following features:

$$\boldsymbol{\Phi}^i(t,\tau)\boldsymbol{\Phi}^i(\tau,t_0)=\boldsymbol{\Phi}^i(t,t_0),\quad\left[\boldsymbol{\Phi}^i(t,\tau)\right]^{-1}=\boldsymbol{\Phi}^i(\tau,t) \tag{21}$$

In the actual computation process, discretization needs to be implemented for equation (19):

$$\delta\boldsymbol{x}_k^i=\boldsymbol{\Phi}^i(t_k,t_{k-1})\delta\boldsymbol{x}_{k-1}^i+\boldsymbol{G}\int_{t_{k-1}}^{t_k}\boldsymbol{\Phi}^i(t_k,\tau)\boldsymbol{w}_{k-1}^i(\tau)\mathrm{d}\tau \tag{22}$$

In a sampling interval from t_{k-1} to t_k, the white noise $\mathbf{w}_{k-1}^i(\tau)$ can be considered as a constant. The integral coefficient denotes that:

$$\boldsymbol{G}_k^i=\boldsymbol{G}\int_{t_{k-1}}^{t_k}\boldsymbol{\Phi}(t_k,\tau)\mathrm{d}\tau \tag{23}$$

Preprints (www.preprints.org) | NOT PEER-REVIEWED | Posted: 24 January 2019 doi:10.20944/preprints201901.0243.v1

For simplicity, the white noise will be denoted as $\boldsymbol{w}_{k-1}^{i}$ in the following paper. Then the discretized state equation derived from equation (22) is:

$$\delta \boldsymbol{x}_k^i = \boldsymbol{\Phi}_{k-1}^i \delta \boldsymbol{x}_{k-1}^i + \boldsymbol{G}_k^i \boldsymbol{w}_{k-1}^i \tag{24}$$

In which, $\boldsymbol{\Phi}_{k-1}^{i}$ denotes the state transition matrix from t_{k-1} to t_k. According to equation (24), the predicted state covariance matrix is

$$\bar{\boldsymbol{P}}_k^i = \boldsymbol{\Phi}_{k-1}^i \hat{\boldsymbol{P}}_{k-1}^i \boldsymbol{\Phi}_{k-1}^{i\,\mathrm{T}} + \boldsymbol{G}_{k-1}^i \boldsymbol{Q}_{k-1}^i \boldsymbol{G}_{k-1}^{i\,\mathrm{T}} \tag{25}$$

4. Whole-Constellation Centralized Extended Kalman Filter

The whole-constellation centralized extended Kalman filter (WCCEKF) is one of the centralized data processing method. According to this method, a main satellite and a back-up satellite are assigned to complete the task of data processing. The other satellites in the constellation need to send their measurement data, state vectors and corresponding covariance matrices to the main satellite for orbit determinations.

For all the satellites in the constellation, the states and corresponding improving values from equations (1) and (2) are collected and stored in a state vector $\boldsymbol{X}_k$ and an improving values vector $\delta \boldsymbol{x}_k$ [6, 28]:

$$\boldsymbol{X}_k = \left[(\boldsymbol{X}^1)^T \quad (\boldsymbol{X}^2)^T \quad \cdots \quad (\boldsymbol{X}^i)^T \quad \cdots \quad (\boldsymbol{X}^n)^T \right]^{\mathrm{T}} \tag{26}$$

$$\delta \boldsymbol{x}_k = \left[(\delta \boldsymbol{x}_k^1)^T \quad (\delta \boldsymbol{x}_k^2)^T \quad \cdots \quad (\delta \boldsymbol{x}_k^i)^T \quad \cdots \quad (\delta \boldsymbol{x}_k^n)^T \right]^{\mathrm{T}} \tag{27}$$

where n is the number of satellites in the system. In this way, the state equation for all the satellites can be obtained through Equation (24):

$$\delta \boldsymbol{x}_k = \boldsymbol{\Phi}_{k-1} \delta \boldsymbol{x}_{k-1} + \boldsymbol{G}_k \boldsymbol{w}_{k-1} \tag{28}$$

State transition matrix $\boldsymbol{\Phi}_k$ and integral coefficient matrix $\boldsymbol{G}_k$ are diagonal matrices and can be expressed as:

$$\boldsymbol{\Phi}_{k-1} = diagonal\left[(\boldsymbol{\Phi}_{k-1}^1) \quad (\boldsymbol{\Phi}_{k-1}^2) \quad \cdots \quad (\boldsymbol{\Phi}_{k-1}^i) \quad \cdots \quad (\boldsymbol{\Phi}_{k-1}^n) \right] \tag{29}$$

$$\boldsymbol{G}_k = diagonal\left[(\boldsymbol{G}_k^1) \quad (\boldsymbol{G}_k^2) \quad \cdots \quad (\boldsymbol{G}_k^i) \quad \cdots \quad (\boldsymbol{G}_k^n)^T \right] \tag{30}$$

State noise vector, w_{k-1}, stores the noise for all the satellites in the constellation:

$$w_{k-1} = \left[(w_{k-1}^1) \quad (w_{k-1}^2) \quad \cdots \quad (w_{k-1}^j) \quad \cdots \quad (w_{k-1}^n) \right]^{\mathrm{T}} \tag{31}$$

and it has the statistical characteristics as follows:

$$E\left[\boldsymbol{w}_{k-1} \right] = 0, \quad E\left[\boldsymbol{w}_{k-1}^i (\boldsymbol{w}_{k-1}^j)^T \right] = \begin{cases} \boldsymbol{Q}_{k-1}^i & i = j \\ 0 & i \neq j \end{cases} \tag{32}$$

$$E\left[\boldsymbol{w}_{k-1} \boldsymbol{w}_{k-1}^T \right] = \boldsymbol{Q}_{k-1} = diagonal\left[\boldsymbol{Q}_{k-1}^1 \quad \boldsymbol{Q}_{k-1}^2 \quad \cdots \quad \boldsymbol{Q}_{k-1}^i \quad \cdots \quad \boldsymbol{Q}_{k-1}^n \right] \tag{33}$$

The measurement equation which is a combination of equations (8) and (12) is then derived as:

$$z_k = \boldsymbol{H}_k \delta \boldsymbol{x} + \varepsilon_k \tag{34}$$

where $\boldsymbol{H}_k = [\boldsymbol{0} \cdots (\boldsymbol{H}^i)^{\mathrm{T}} \cdots \boldsymbol{0} \cdots (\boldsymbol{H}^j)^{\mathrm{T}} \cdots \boldsymbol{0}]^{\mathrm{T}}$, $z_k = z_k^{ij}(t_{\mathrm{k}}), \varepsilon_k = \varepsilon^{ij}(t_{\mathrm{k}})$ for i$^{\mathrm{th}}$ satellite and j$^{\mathrm{th}}$ satellite with ISL; $\boldsymbol{H}_k = [\boldsymbol{0} \cdots (\boldsymbol{H}^i)^{\mathrm{T}} \cdots \quad \boldsymbol{0}]^{\mathrm{T}}$, $z_k = z_k^{ig}(t_{\mathrm{k}})$, $\varepsilon_k = \varepsilon^{ig}(t_{\mathrm{k}})$ for GAS to i$^{\mathrm{th}}$ satellite

Preprints (www.preprints.org) | NOT PEER-REVIEWED | Posted: 24 January 2019 doi:10.20944/preprints201901.0243.v1

measurement. Next, a measurement covariance matrix $R_k = \mathrm{E}(\varepsilon_k \varepsilon_k^T)$, an initial state vector $\bar{\boldsymbol{X}}_0 = \mathrm{E}(\boldsymbol{X}_0^*)$ and an initial state vector covariance $\bar{\boldsymbol{P}}_0 = \mathrm{E}[\boldsymbol{X}_0^* \boldsymbol{X}_0^{*\mathrm{T}}]$ are defined. Finally, the method of WCCEKF that combines the satellite-to-satellite measurements and satellite-to-GAS measurements can be expressed as [29]:

$$\bar{\boldsymbol{P}}_k = \boldsymbol{\Phi}_{k-1} \hat{\boldsymbol{P}}_{k-1} \boldsymbol{\Phi}_{k-1}^{\mathrm{T}} + \boldsymbol{G}_{k-1} \boldsymbol{Q}_{k-1} \boldsymbol{G}_{k-1}^{\mathrm{T}} \tag{35}$$

$$\boldsymbol{K}_k = \bar{\boldsymbol{P}}_k \boldsymbol{H}_k^{\mathrm{T}} \left(\boldsymbol{H}_k^{\mathrm{T}} \bar{\boldsymbol{P}}_k \boldsymbol{H}_k + \boldsymbol{R}_k \right)^{-1} \tag{36}$$

$$\delta \hat{x}_k = \boldsymbol{K}_k z_k \tag{37}$$

$$\hat{\boldsymbol{X}}_k = \bar{\boldsymbol{X}}_k + \delta \hat{x}_k \quad \hat{\boldsymbol{X}}_k = \bar{\boldsymbol{X}}_k + \delta \hat{x}_k \tag{38}$$

$$\hat{\boldsymbol{P}}_k = \left(\boldsymbol{I} - \boldsymbol{K}_k \boldsymbol{H}_k \right) \bar{\boldsymbol{P}}_k \tag{39}$$

The dimension of state vector $\boldsymbol{X}_k$ is

$$N_W = 6n + \sum_{i=1}^{n} D^i \tag{40}$$

where D^i is the number of dynamic parameters for the i[th] satellite.

In the method of WCCEKF, each satellite is correlated with the other satellites through the state vector covariance matrix which has the dimension of $N_W \times N_W$. What is more, matrix $(\boldsymbol{H}_k^{\mathrm{T}} \bar{\boldsymbol{P}}_k \boldsymbol{H}_k + \boldsymbol{R}_k)$ with the dimension of $m \times m$ (m is the dimension of the measurement vector) needs to be inversed during the process and a huge computational amount is expected. The computation amount for a process of WCCEKF is:

$$4N_W^2 (N_W^2 - 1) + (N_W - 1) N_W (N_W + 1) / 6 + (2N_W^2 + 7N_W + 1) \times m \tag{41}$$

If the WCCEKF algorithm is employed, the on-board computer of the main satellite would need to process all the ISL measurement and satellite-to-GAS measurement data to finish the task of orbit determination and navigation message generation for satellites in the constellation. Due to the huge computation amount and great complexity of communication, WCCEKF is difficult to be implemented in a satellite constellation with limited on-board computation ability.

In addition, the WCCEKF is also vulnerable. Once the main satellite and its backup satellite failed, the entire navigation constellation would stop working. To avoid the drawbacks in the WCCEKF method, many researches nowadays are focusing on developing the distributed data processing algorithm.

5. Distributed Orbit Determination

For the distributed orbit determination algorithms based on the ISL, data processing is assigned to each satellite. In this process, each satellite collects the ISLs measurement data with respect to its visible satellite and estimates the self-related state vectors.

5.1. Reduced-Order Iterative Cascade EKF

Preprints (www.preprints.org) | NOT PEER-REVIEWED | Posted: 24 January 2019 doi:10.20944/preprints201901.0243.v1

For i[th] and j[th] satellites with ISL measurements, the iterative cascade EKF (ICEKF) [12] assumes that the state vector X^j of j[th] satellite is known. Thus, the measurement equation which is similar to equation (34) is derived as:

$$z_k^i = \boldsymbol{H}_k^i \delta \boldsymbol{x}_k^i + \varepsilon_k^i \tag{42}$$

For ISL measurement, the innovation is $z_k^i = z_k^{ij}(t_k)$, the measurement error is $\varepsilon_k^i = \boldsymbol{H}_k^j \delta \boldsymbol{x}_k^j + \varepsilon^{ij}(t_k)$ and measurement covariance matrix is $R_k^i = E[\varepsilon_k^i(\varepsilon_k^i)^T] = E[\varepsilon^{ij}(t_k)\varepsilon^{ij}(t_k)^T] = R_{k,ISL}^i$. For satellite-to-GAS measurement, the innovation is $z_k^i = z_k^{ig}(t_k)$, the measurement error is $\varepsilon_k^i = \varepsilon^{ig}(t_k)$, and measurement covariance matrix is $R_k^i = E(\varepsilon_k^i(\varepsilon_k^i)^T] = E(\varepsilon^{ig}(t_k)\varepsilon^{ig}(t_k)^T] = R_{k,GAS}^i$. An initial state vector $\bar{\boldsymbol{X}}_0^i = \mathrm{E}(\boldsymbol{X}_0^{i*})$ and an initial state vector covariance matrix $\bar{\boldsymbol{P}}_0^i = \mathrm{E}[\boldsymbol{X}_0^{i*}\boldsymbol{X}_0^{i*\mathrm{T}}]$ are defined. Result from the method of ICEKF that combines the ISL measurement and satellite-to-GAS measurement can be obtained as:

$$\bar{\boldsymbol{P}}_k^i = \boldsymbol{\Phi}_{k-1}^i \hat{\boldsymbol{P}}_{k-1}^i \boldsymbol{\Phi}_{k-1}^{i\mathrm{T}} + \boldsymbol{G}_{k-1}^i \boldsymbol{Q}_{k-1}^i \boldsymbol{G}_{k-1}^{i\mathrm{T}} \tag{43}$$

$$\boldsymbol{K}_k^i = \bar{\boldsymbol{P}}_k^i \boldsymbol{H}_k^{i\mathrm{T}} \left(\boldsymbol{H}_k^{i\mathrm{T}} \bar{\boldsymbol{P}}_k^i \boldsymbol{H}_k^i + \boldsymbol{R}_k^i \right)^{-1} \tag{44}$$

$$\delta \hat{x}_k^i = \boldsymbol{K}_k^i z_k^i \tag{45}$$

$$\hat{\boldsymbol{X}}_k^i = \bar{\boldsymbol{X}}_k^i + \delta \hat{x}_k^i \tag{46}$$

$$\hat{\boldsymbol{P}}_k^i = \left(\boldsymbol{I} - \boldsymbol{K}_k^i \boldsymbol{H}_k^i \right) \bar{\boldsymbol{P}}_k^i \tag{47}$$

In this way, only local state vector related to the i[th] satellite itself is included in the measurement equation. The dimension of state vector $\boldsymbol{X}_k^i$ is:

$$N_i = 6 + D^i \tag{48}$$

The computation amount for ICEKF algorithm is:

$$4N_i^2(N_i^2 - 1) + (N_i - 1)N_i(N_i + 1)/6 + (2N_i^2 + 7N_i + 1) \times (m/n) \tag{49}$$

As a result, the computational complexity is greatly reduced. However, the state vector of the i[th] satellite is only correlated with the measurement of itself and this method must be referred to as a reduced-order suboptimal filter. In order to improve the filtering accuracy, a common approach is to iterate the process above till convergence. In a data frame, after receiving the state vectors of the other visible satellites, the i[th] satellite will update its own state vectors and covariance matrix by equations (42)~(47). Other satellites will do the same process in turn and iterate until the state vector of each satellite is converged.

However, the method of ICEKF assumes that the state vectors of the other satellites have no errors, but this is not the case. In such way, the method of ICEKF needs an uncertain number of iterations to approach convergence. In a constellation with large number of satellites, reaching convergence could be time-consuming [12, 13].

5.2. Reduced-Order Increased Measurement Covariance EKF

Preprints (www.preprints.org) | NOT PEER-REVIEWED | Posted: 24 January 2019 doi:10.20944/preprints201901.0243.v1

To accelerate the data-processing in the ICEKF method, the reduced-order increased measurement covariance EKF（IMCEFK）[12] is carried out. This method includes the error of the state vectors of the jth satellite into the measurement covariance matrix R_k^i between ith satellite and jth satellite. Let us regenerate the ISL measurement error in equation (42) as $\boldsymbol{\varepsilon}_k^i = \boldsymbol{H}^j \delta \boldsymbol{x}_k^j + \varepsilon^{ij}(t_k)$, then the corresponding measurement covariance matrix is:

$$\begin{aligned} \mathrm{E}\left[\boldsymbol{\varepsilon}_k^i \boldsymbol{\varepsilon}_k^{i\,\mathrm{T}}\right] &= \mathrm{E}\left[(\boldsymbol{H}_k^j \delta \boldsymbol{x}_k^j + \varepsilon^{ij}(t_k))(\boldsymbol{H}_k^j \delta \boldsymbol{x}_k^j + \varepsilon^{ij}(t_k))^{\mathrm{T}}\right] \\ &= \boldsymbol{H}_k^{\mathrm{j}} \overline{\boldsymbol{P}}_k^{\mathrm{j}} \boldsymbol{H}_k^{\mathrm{jT}} + R_k^i \end{aligned} \tag{50}$$

in which $\overline{\boldsymbol{P}}_k^{\mathrm{j}}$ is the state vector covariance matrix of jth satellite. Equation (50) implies that ISL measurements contains not only the measurement errors, but also the jth satellite state vector error, thus the measurement covariance matrix is assembled as:

$$R_{k\ assembled}^i = \boldsymbol{H}_k^{\mathrm{j}} \overline{\boldsymbol{P}}_k^{\mathrm{j}} \boldsymbol{H}_k^{\mathrm{jT}} + R_k^i \tag{51}$$

the subscripts, *assembled*, indicates that it is an assembled measurement covariance matrix.

Next, the R_k^i in equation (44) is replaced by $R_{k\ amp}^i$, and the gain matrix becomes

$$\boldsymbol{K}_k^i = \overline{\boldsymbol{P}}_k^i \boldsymbol{H}_k^{\mathrm{i\,T}} \left(\boldsymbol{H}_k^{\mathrm{i\,T}} \overline{\boldsymbol{P}}_k^i \boldsymbol{H}_k^{\mathrm{i}} + \boldsymbol{H}_k^j \overline{\boldsymbol{P}}_k^{\mathrm{j}} \boldsymbol{H}_k^{\mathrm{jT}} + \boldsymbol{R}_k^i \right)^{-1} \tag{52}$$

After repeating the steps in equations (42), (43), (51), (45), (46), and (47), the orbits for ith satellites are determined. In this way, a reduction of the number of the iterations is expected. The computation amount of IMCEKF is:

$$4N_i^2(N_i^2-1) + (N_i-1)N_i(N_i+1)/6 + (2N_i^2+7N_i+1) \times (m/n) \tag{53}$$

In some situations, iteration may not be required [18]. To summarize, compared to ICEKF, the IMCEKF is a reduced-order approach and needs to transmit not only the local state vector but also its covariance matrix to the other satellites.

5.3. Balanced Extended Kalman Filter

In one computation cycle, the ICEKF and IMCEKF algorithm only improve the state vector on one end of the ISL. To increase the efficiency and accuracy, the balanced extended Kalman filter (BEKF) is proposed. For ith and jth satellite, the satellites state vectors on the both ends of the ISL can be improved simultaneously. To keep the balance of the accuracy increments on both satellites, the improving state vectors should be adjusted by:

$$\left(\overline{\boldsymbol{P}}_k^i\right)^{-1} \delta \hat{\boldsymbol{x}}_k^i = \left(\overline{\boldsymbol{P}}_k^j\right)^{-1} \delta \hat{\boldsymbol{x}}_k^j \tag{54}$$

With the constraint of the equation (54), the BEKF can be derived from equations (8), (12) and (24), and it can be completed by following steps:

$$\overline{\boldsymbol{P}}_k^i = \boldsymbol{\Phi}_{k-1}^i \hat{\boldsymbol{P}}_{k-1}^i \boldsymbol{\Phi}_{k-1}^{\mathrm{i\,T}} + \boldsymbol{G}_{k-1}^i \boldsymbol{Q}_{k-1}^i \boldsymbol{G}_{k-1}^{\mathrm{i\,T}} \tag{55}$$

$$\overline{\boldsymbol{P}}_k^j = \boldsymbol{\Phi}_{k-1}^j \hat{\boldsymbol{P}}_{k-1}^j \boldsymbol{\Phi}_{k-1}^{\mathrm{j\,T}} + \boldsymbol{G}_{k-1}^j \boldsymbol{Q}_{k-1}^i \boldsymbol{G}_{k-1}^{\mathrm{j\,T}} \tag{56}$$

$$N_B = \begin{bmatrix} H_k^i R^{-1} H_k^i + \left(\overline{\boldsymbol{P}}_k^i\right)^{-1} & H_k^{iT} R^{-1} H_k^j \\ H_k^{jT} R^{-1} H_k^i & H_k^{jT} R^{-1} H_k^j + \left(\overline{\boldsymbol{P}}_k^j\right)^{-1} \end{bmatrix} \tag{57}$$

Preprints (www.preprints.org) | NOT PEER-REVIEWED | Posted: 24 January 2019 doi:10.20944/preprints201901.0243.v1

$$C=\left[\left(\bar{\boldsymbol{P}}_k^i\right)^{-1} \quad -\left(\bar{\boldsymbol{P}}_k^j\right)^{-1}\right] \tag{58}$$

$$N_C = CN_B^{-1}C^{\mathrm{T}} \tag{59}$$

$$M_C = N_B^{-1}C^{\mathrm{T}}N_C^{-1}C \tag{60}$$

$$\boldsymbol{K}_k^{ij} = (I-M)\begin{bmatrix}\bar{\boldsymbol{P}}_k^i \boldsymbol{H}_k^{\mathrm{i\,T}} \\ \bar{\boldsymbol{P}}_k^j \boldsymbol{H}_k^{\mathrm{j\,T}}\end{bmatrix}\left[\boldsymbol{H}_k^{\mathrm{i}}\bar{\boldsymbol{P}}_k^i\boldsymbol{H}_k^{\mathrm{i\,T}} + \boldsymbol{H}_k^j\bar{\boldsymbol{P}}_k^j\boldsymbol{H}_k^{j\,\mathrm{T}} + \boldsymbol{R}_k^i\right]^{-1} \tag{61}$$

(62)

$$\begin{bmatrix}\delta\hat{x}_k^i \\ \delta\hat{x}_k^j\end{bmatrix} = \boldsymbol{K}_k z_k^i \tag{63}$$

$$\begin{bmatrix}\hat{\boldsymbol{X}}_k^i \\ \hat{\boldsymbol{X}}_k^j\end{bmatrix} = \begin{bmatrix}\bar{\boldsymbol{X}}_k^i \\ \bar{\boldsymbol{X}}_k^j\end{bmatrix} + \begin{bmatrix}\delta\hat{x}_k^i \\ \delta\hat{x}_k^j\end{bmatrix} \tag{64}$$

$$\begin{bmatrix}\hat{\boldsymbol{P}}_k^i & \hat{\boldsymbol{P}}_k^{ij} \\ \hat{\boldsymbol{P}}_k^{ji} & \hat{\boldsymbol{P}}_k^j\end{bmatrix} = \left\{I - K_K\begin{bmatrix}\boldsymbol{H}_k^{\mathrm{i}} & \boldsymbol{H}_k^{\mathrm{j}}\end{bmatrix}\right\}\begin{bmatrix}\bar{\boldsymbol{P}}_k^i & 0 \\ 0 & \bar{\boldsymbol{P}}_k^j\end{bmatrix} - M\begin{bmatrix}\bar{\boldsymbol{P}}_k^i & 0 \\ 0 & \bar{\boldsymbol{P}}_k^j\end{bmatrix} \tag{65}$$

The dimension of state vector $\boldsymbol{X}_k^i$ and $\boldsymbol{X}_k^j$ of i[th] and j[th] satellites is

$$N_{ij} = 12 + \sum_{i=1}^{n}(D^i + D^j) \tag{66}$$

The computation amount of BEKF is:

$$4N_i^2(N_i^2-1) + (N_i-1)N_i(N_i+1)/6 + (2N_{ij}^2 + 7N_{ij} + 1)\times(m/2n) \tag{67}$$

The method has the following features:

(1) The method of BEKF collects the data of ISL measurements, satellite-to-GAS measurements (if it is available), and the satellite state vectors and their covariance matrices on both ends of the ISL. After the calculation of the BEKF algorithm, the improved state vectors and their covariance matrices are sent to the other visible satellites. The BEKF method modifies the denominator of gain matrix from $\boldsymbol{K}_k^{ij}$ to $\boldsymbol{H}_k^{\mathrm{i}}\bar{\boldsymbol{P}}_k^i\boldsymbol{H}_k^{\mathrm{i\,T}} + \boldsymbol{H}_k^j\bar{\boldsymbol{P}}_k^j\boldsymbol{H}_k^{j\,\mathrm{T}} + \boldsymbol{R}_k^i$ which is similar to the method of IMCEKF. Furthermore, it modifies the gain matrix by a factor of $(I-M_C)$. Therefore, the BEKF algorithm is expected to yield results with higher precision.

(2) It seems that BEKF requires more ISL processes than the other EKFs. In fact, the state vectors and their covariance matrices on both ends are improved at the same time. It is unnecessary to repeat the ISL process for the same two satellites. The computation load of BEKF is similar to that of IMCEKF.

(3) Iteration process that is implemented in the ICEFK algorithm is not required in the BEKF method to achieve high accuracy.

Preprints (www.preprints.org) | NOT PEER-REVIEWED | Posted: 24 January 2019 doi:10.20944/preprints201901.0243.v1

(4) The improving state vectors are balanced in such that the satellite with lower state precision will have more increments on the accuracy while the satellite with higher state precision will have less adjustments.

(5) Compared to the other EKFs, in equation (65), the state vectors covariance matrices of the two satellites are subtracted with $M_C\begin{bmatrix}\bar{\boldsymbol{P}}_k^i & 0\\ 0 & \bar{\boldsymbol{P}}_k^j\end{bmatrix}$. Therefore, the values in the matrices are reduces and the accuracy of the state vectors is improved.

(6) The two satellites are correlated by $\hat{\boldsymbol{P}}_k^{ij}$ and $\hat{\boldsymbol{P}}_k^{ji}$ in equation (65), however, these two matrices have to be ignored in this distributed filter. As a result, the current method should be categorized as a reduced-order sub-optimal orbit determination method.

6. Simulations and Analyses

In order to compare the performance of abovementioned methods, navigation constellation simulations are carried out with the parameters of Walker 24/3/2:55°, 22116 kilometers [30]. The dynamic model applied to satellite orbit are:

1) The earth's gravitational effects of 70×70,
2) The lunar, solar and other planetary gravitational perturbations,
3) The solar radiation pressure,
4) The other general relativistic forces.

The eighth-order Runge-Kutta method is employed for orbit integration. IERS96 model is adopted for the Earth Orientation Parameters [31]. Besides, TDMA mode is adopted in ISL with measurement frames and data transmitting frames. The total error of Ka-band ISL PR is 0.5 meters (1 σ). To avoid ground atmospheric disturbance, the ISLs with a vertical distance less than 1000 kilometers to the Earth surface are not considered. Eight GASs that are located in Xiamen, Kashi, Beijing, Lhasa, Sanya, Urumqi, Jiamusi, and Xi'an in China are set up in the simulation. With a minimum elevation of 10°, the Hopfield / Marini model [1] is employed in tropospheric delay correction for the satellite-to-GAS PR which has a total error of 3 meters (1 σ).

The impact of complex factors is not considered in the simulations. In addition, the ISL PR measurement noise is assumed to be normally distributed without pollution to have better comparisons for the different algorithms.

The orbit determination simulations are carried out in two steps:

(1) An analytical orbit is generated and the corresponding ISL and satellite-to-GAS PRs are calculated.

(2) Using the abovementioned PRs, the satellite orbits are calculated by the different methods and compared with the analytical orbit to find out orbit determination precisions.

The position error, radial error, along track error, and cross track error versus time normalized by day for satellite SV-01 computed from different methods are presented in Figure 1 to Figure 4. It should be noted that errors from the other satellites in the constellation are excluded in present analysis since the errors are similar to that of satellite SV-01.

Preprints (www.preprints.org) | NOT PEER-REVIEWED | Posted: 24 January 2019 doi:10.20944/preprints201901.0243.v1

389

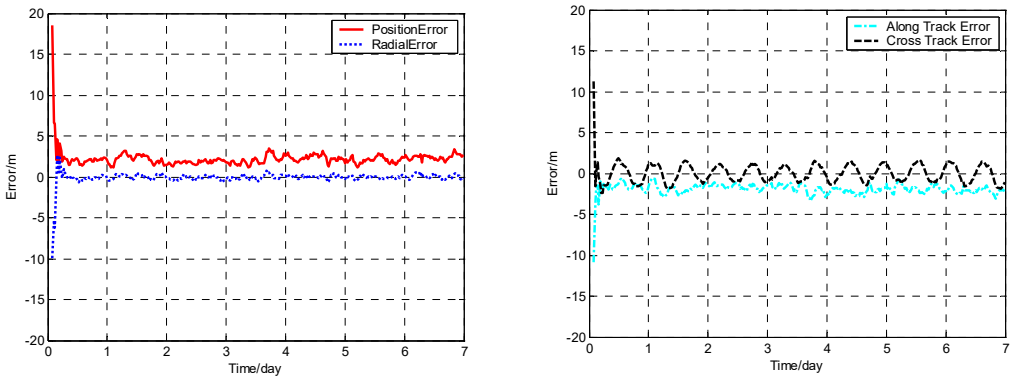

(a) (b)

Figure 1. Orbit determination errors of SV-01 by WCCEKF algorithm

390

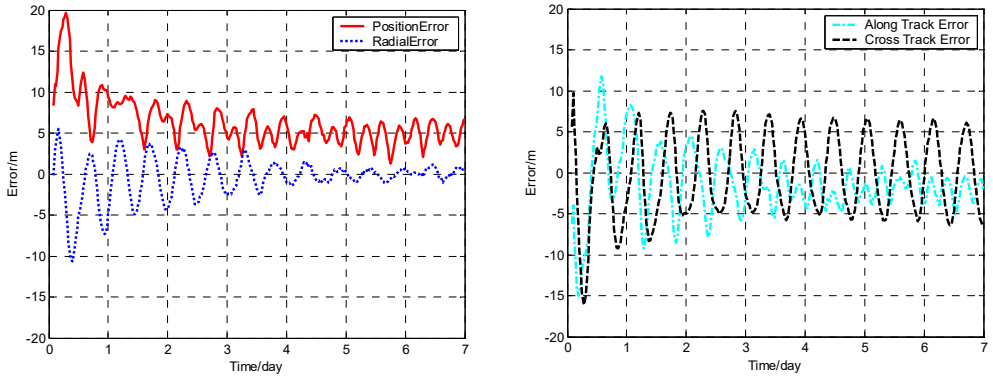

(a) (b)

Figure 2. Orbit determination errors of SV-01 by ICEKF algorithm

391

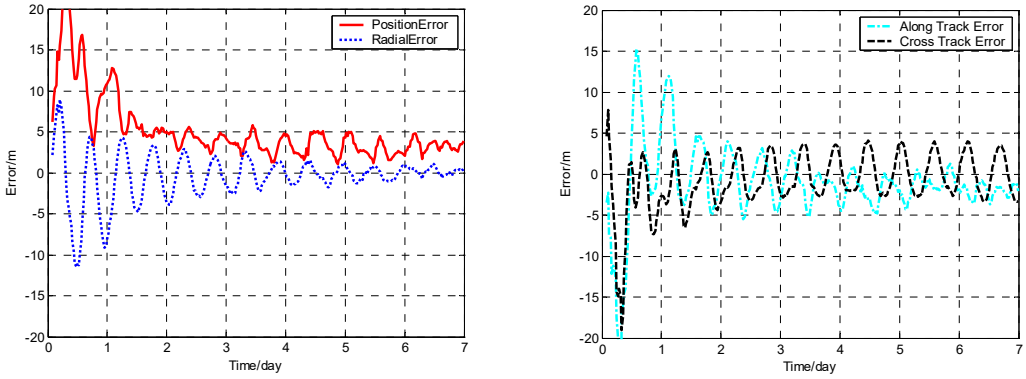

(a) (b)

Figure 3. Orbit determination errors of SV-01 by IMCEKF algorithm

Preprints (www.preprints.org) | NOT PEER-REVIEWED | Posted: 24 January 2019 doi:10.20944/preprints201901.0243.v1

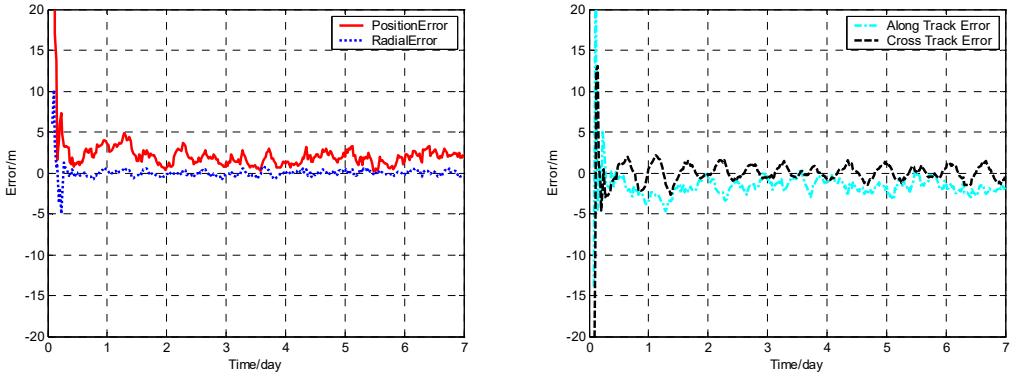

(a) (b)

Figure 4. Orbit determination errors of SV-01 by BEKF algorithm

For each method, the orbit determination errors tend to oscillate steadily after poor initial results. However, differences can be observed among four algorithms. To have quantitative comparisons, the root mean square (RMS) of different errors from each method is calculated in stable section. The average RMS for position error, radial error, along-track error, and cross track error from the four methods are shown in Figure 5. It is worth to point out that the average RMS of position error for WCCEKF, ICEKF, IMCEKF, and BEKF algorithms is around 1.6 meters, 4.5 meters, 2.9 meters, and 1.9 meters, respectively.

Next, the computation amounts for different methods are summarized in Table 1 and visualized in Figure 6.

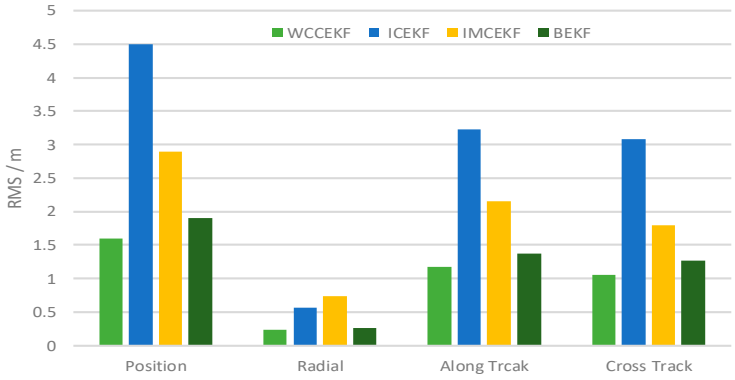

Figure 5. Average RMS of orbit errors

Table 1. Computation amounts, unit: FLOPS (floating-point operations per second）

Methods	Computation amount (FLOPS: floating-point operations per second）
WCCEKF	$4N_W^2(N_W^2-1)+(N_W-1)N_W(N_W+1)/6+(2N_W^2+7N_W+1)\times m$
ICEKF or IMCEKF	$4N_i^2(N_i^2-1)+(N_i-1)N_i(N_i+1)/6+(2N_i^2+7N_i+1)\times(m/n)$
BEKF	$4N_i^2(N_i^2-1)+(N_i-1)N_i(N_i+1)/6+(2N_{ij}^2+7N_{ij}+1)\times(m/2n)$

Preprints (www.preprints.org) | NOT PEER-REVIEWED | Posted: 24 January 2019 doi:10.20944/preprints201901.0243.v1

Figure 6. Computation amounts

The WCCEKF algorithm yields the optimal results with the highest precision. Among the three distributed orbit determination algorithms (ICEKF, IMCEKF, and BEKF), highest orbit estimation precision can be observed in the method of BEKF. When it comes to the computation amounts for the four method in Table 1 and Figure 6, the largest calculation amount is required in WNCEKF algorithm of which the orbit accuracy is the best. In the methods of ICEKF, IMCEKF, and BEKF with sub-optimal distributed orbit determination, significant reductions of the computation amount can be observed when compared to in the method of WNCEKF.

Finally, the performances of the WCCEKF, ICEKF, IMCEKF, and BEKF algorithms in are summarized and provided in Table 2 in different respects.

Table 2. Comparisons of performances

Algorithm	Description	Computation amount	Orbital accuracy
WCCEKF	Whole-constellation centralized EKF	Maximum	Best
ICEKF	Iterative Cascade EKF	Minimum	Normal
IMCEKF	Increased measurement covariance EKF	Minimum	Normal
BEKF	Balanced EKF	Minimum	Better

7. Conclusion

The fundamental theory of satellite orbit determination for autonomous navigation is introduced. Four algorithms for autonomous navigation with onboard data processing, i.e. whole-constellation centralized extended Kalman filter (WCCEKF), iterative cascade extended Kalman filter (ICEKF), increased measurement covariance extended Kalman filter (IMCEKF), and balanced extended Kalman filter (BEKF), are illustrated. The WCCEFK technique processes the measurement data for orbit determination by a main satellite while the other three algorithms distribute the computation on every satellite in the constellation. The simulation results show that the method WCCEKF has the optimal orbit determination accuracy among the four methods but demands the largest computation loads. Similar computation amounts are observed in the three distributed algorithms. Compare to ICEKF technique, covariance matrices of the other satellites are absorbed into the measurement covariance matrix in the method of IMCEKF. As a result, a smaller orbit error is observed in the IMCEKF algorithm than in the ICEKF. Since the BEKF method estimates the state vectors of the satellites on both ends of the ISL in a balanced mean and increases their accuracy simultaneously, this method yields the best results among the three distributed estimation algorithms. The BEKF can be considered as an appropriate distributed data processing algorithm for a GNSS.

Author Contributions: Yuanlan Wen conceived the idea with Xiufeng He; Jun Zhu, Youxing Gong and Qian Wang verified the feasibility of the proposed method and implemented different algorithms in the simulations; Yuanlan Wen and Jun Zhu analyzed the simulation results; Yuanlan Wen and Youxing Gong wrote the first version of the manuscript.

Funding: This research is supported by the Fundamental Research Funds in the Central Universities (grant number 2018B07414).

Acknowledgments: We would like to thank the anonymous reviewers and members of the editorial team for their comments and contributions.

Conflicts of Interest: The authors declare no conflict of interest.

References

1. Kaplan, E. D.; Hegarty, C. J., *Understanding GPS: principles and application(Second Edition)*. Norwood, MA 02062: ARTECH HOUSE, INC: 2006.
2. Hofmannwellenhof, B., *GNSS -- global navigation satellite systems : GPS, GLONASS, Galileo, and more*. Springer Wien: 2008, 647-651.
3. Rajan J A, B. P., Orr M, On-orbit validation of GPS IIR autonomous navigation. In *Proceedings of the ION 59th Annual Meeting, Albuquerque, NM*, 2003, 411-419.
4. Zhu, J. Research on Orbit Determination and Time Synchronizing Method of Navigation Satellite Based on Crosslinks. National University of Defense Technology, 2011.
5. Hang, Y. I.; Bo, X. U., Long-term semi-autonomous orbit determination supported by a few ground stations for navigation constellation. *Science China Physics Mechanics & Astronomy* **2011,** 54, (7), 1342-1353.
6. WEN, Y.; ZHU, J.; LI, Z.; LIAO, Y., Simulation and Analysis of Integrated Orbit Determination of Satellites Constellation. *Journal of Astronautics* **2009,** 30, (1), 155-163.
7. Ananda, M. P.; Bernstein, H.; Cunningham, K. E.; Feess, W. A.; Stroud, E. G., Global Positioning System (GPS) autonomous navigation. In *IEEE Position Location & Navigation Symposium*, 2002.
8. Fisher, S. C.; Ghassemi, K., GPS IIF-the next generation. In *Proceedings of the IEEE*, 1999; Vol. 87, 24-47.
9. Luba, O.; Boyd, L.; Gower, A.; Crum, J., GPS III system operations concepts. *IEEE Aerospace & Electronic Systems Magazine* **2005,** 20, (1), 10-18.
10. Eissfeller, B.; Zink, T.; Wolf, R.; Hammesfahr, J.; Hornbostel, A.; Hahn, J. H.; Tavella, P., Autonomous satellite state determination by use of two-directional links. *International Journal of Satellite Communications* **2010,** 18, (4-5), 325-346.
11. Mandic, M.; Breger, L.; How, J. P., Analysis of Decentralized Estimation Filters for Formation Flying Spacecraft. *Bridging Social Psychology* **2006**.
12. Ferguson, P. A. Distributed estimation and control technologies for formation flying spacecraft. Massachusetts Institute of Technology, 2003.
13. Park, C. W. Precise relative navigation using augmented CDGPS. Stanford University, 2001.
14. GPS Dancer project: http://www.gpsdancer.org
15. Chen, Y.; Hu, X.; Zhou, S.; Song, X.; Huang, Y.; Mao, Y.; Huang, C.; Chang, Z.; Wu, S., A new autonomous orbit determination algorithm based on inter-satellite ranging measurements. *SCIENTIA SINICA Physica, Mechanica & Astronomica* **2015,** 45, (7), 079511: 1-8

16. Yang, D.; Yang, J.; Li, G.; Zhou, Y.; Tang, C. P., Globalization highlight: orbit determination using BeiDou inter-satellite ranging measurements. *GPS Solutions* **2017,** 21, (3), 1395-1404.
17. Huang, F.; Huang, W.; Wang, Y.; Zhou, Y.; Lin, K., Analysis of Ground Anchor Stations' Influence on Autonomous Orbit Determination with Distributed Algorithm. In *China Satellite Navigation Conference*, Changsha, 2016.
18. Kai, X.; Wen, Y.; Ying, L.; Song, Y.; Su, T.; Zhi, Z., Distributed Orbit Determination Based on Increased Measurement Covariance EKF for Global Navigation Satellite System with Inter-satellite Link. In *China Satellite Navigation Conference*, Nanjing, 2015.
19. Zhou, Y.; Lai, J.; Zhou, Y.; Lin, J.; Yang, N.; Yang, J., Cooperative simultaneous autonomous orbit determination and time synchronization: A distributed factor graph approach. In *IEEE International Workshop on Signal Processing Advances in Wireless Communications*, 2017.
20. Wang, H.; Chen, Z.; Zheng, J.; Chu, H., A New Algorithm for Onboard Autonomous Orbit Determination of Navigation Satellites. *Journal of Navigation* **2011,** 64, (S1), 162-179.
21. Lina, H.; Maorong, G.; Jiexian, W.; Jens, W.; Harald, S., Experimental study on the precise orbit determination of the BeiDou navigation satellite system. *Sensors* **2013,** 13, (3), 2911-2928.
22. Hongliang, X. U.; Wang, J.; Zhan, X., Autonomous broadcast ephemeris improvement for GNSS using inter-satellite ranging measurements. *Advances in Space Research* **2012,** 49, (6), 1034-1044.
23. Xie, X.; Geng, T.; Zhao, Q.; Liu, J.; Wang, B., Performance of BDS-3: Measurement Quality Analysis, Precise Orbit and Clock Determination. *Sensors* **2017,** 17, (6), 1233, 1–14.
24. Hu, C.; Wang, Q.; Wang, Z.; Hernández, A. M., New-Generation BeiDou (BDS-3) Experimental Satellite Precise Orbit Determination with an Improved Cycle-Slip Detection and Repair Algorithm. *Sensors* **2018,** 18, (5), 1402-1420.
25. Mao, Y.; Wang, Q.; Chao, H.; He, Y., Accuracy analysis of BDS experiment satellite broadcast ephemeris. In *China Satellite Navigation Conference*, 2018.
26. Yang, Y.; Xu, Y.; Li, J.; Cheng, Y., Progress and performance evaluation of BeiDou global navigation satellite system: Data analysis based on BDS-3 demonstration system. *Science China Earth Sciences* **2018,** 61, (5), 614-624.
27. Zhu, J.; Wen, Y.; Chen, Z.; Ying, L., Research on modeling and simulation of semi-autonomous orbit determination for satellite navigation constellation. In *Asia Simulation Conference 2008/the International Conference on System Simulation and Scientific Computing（ICSC)*, 2008.
28. Tang, C. P.; Xiaogong, H. U.; Zhou, S. S.; Pan, J. Y.; Rui, G.; Guangming, H. U.; Zhu, L. F.; Xiaojie, L. I.; Shan, W. U.; Yan, W., Centralized autonomous orbit determination of Beidou navigation satellites with inter-satellite link measurements:preliminary results. *SCIENTIA SINICA Physica, Mechanica & Astronomica* 2017,47,(2), 029501: 1-11.
29. Yang, Y.; Gao, W.; Zhang, X., Robust Kalman filtering with constraints: a case study for integrated navigation. *Journal of Geodesy* **2010,** 84, (6), 373-381.
30. Walker, J. G., Circular orbit patterns providing continuous whole earth coverage. *Journal of the British Interplanetary Society* **1970,** 24, 369-384.
31. Weber, R.; Rothacher, M.; Beutler, G., Contribution of the GPS to monitor Earth Orientation Parameters. *High Frequency to Subseasonal Variations in Earth Rotation* **2000**, 43-51.